

Model verification and assessment of shear-flexure interaction in pile foundations

Anne Lemnitzer^{*1}, Eduardo Núñez^{2a} and Leonardo M. Massone^{3b}

¹Department of Civil Engineering, Univ. of California Irvine, 4135 Eng. Gateway, Irvine, CA, 92697, USA

²Independent Structural Engineer, Santiago, Chile

³Department of Civil Engineering, University of Chile, Santiago, Blanco Encalada 2002, Santiago, Chile

(Received August 20, 2015, Revised June 4, 2016, Accepted June 11, 2016)

Abstract. Fiber models have been developed and applied to various structural elements such as shear walls, beams and columns. Only scarcely have fiber models been applied to circular foundation systems such as cast in drilled holes shafts (CIDH). In pile foundations with constraint head boundary conditions, shear deformations can easily contribute to the lateral pile response. However, soil structure interaction formulations such as the p - y method, commonly used for lateral pile design, do not include structural shear deformations in its traditional derivation method. A fiber model that couples shear and axial-bending behavior, originally developed for wall elements was modified and validated on circular cross sections (columns) before being applied to a 0.61 m diameter reinforced concrete (RC) pile with fixed head boundary conditions. The analytical response was compared to measured test results of a fixed head test pile to investigate the possible impact of pile shear deformations on the displacement, shear, and moment profiles of the pile. Results showed that shear displacements and forces are not negligible and suggest that nonlinear shear deformations for RC piles should be considered for fixed-head or similar conditions. Appropriate sensor layout is recommended to capture shear deformation when deriving p - y curves from field measurements.

Keywords: piles; lateral loading; soil-pile interaction; shear deformations; reinforced concrete

1. Introduction

Shear - Flexure interaction is a main contributor to the failure of reinforced concrete (RC) elements subjected to strong cyclic transverse loading as induced by earthquakes. The interaction is particularly pronounced along structural boundary zones such as fixed end regions along shear walls, beams, columns and RC pile foundations. Kozmidis *et al.* (2014), for example, identified that large amounts of flexural damages observed during the 2010 Maule earthquake in Chile can be attributed to the effect of shear - flexure interaction at the structural boundary zones and explain the specific damage location observed in the field.

*Corresponding author, Professor, E-mail: alemnitz@uci.edu

^aConsulting Engineer, E-mail: enunez.ing@gmail.com

^bProfessor, E-mail: lmassone@ing.uchile.cl

The use of fiber models has become a frequent analytical tool for modeling the structural behavior of concrete elements given their relatively simple discretization while simultaneously offering a time and cost efficient alternative to complicated finite element formulations. In a typical fiber model, the structural member is discretized in fiber (strip) elements that entail the material behavior in form of stress-strain formulations for concrete and steel. First model formulations were based on the Bernoulli-Euler beam theory by having defined curvatures and deformations of the beam section. Through integration of stresses developed over the cross section an interaction between axial forces and bending moments was established (Chan 1982, Scordelis 1984 and Spacone *et al.* 1996). The Timoshenko beam theory was later introduced into fiber models to include the effect of shear forces and deformations. Researchers tried to capture shear effects by superimposing shear and flexural deformations utilizing a truss analogy (e.g., Guedes *et al.* 1994, Martinelli 1998, Ranzo and Petrangeli 1998) or by employing multi-axial constitutive relationships to couple shear-flexure interaction (e.g., Petrangeli *et al.* 1999a, b, Vecchio and Collins 1988, Remino 2004, Kaba and Mahin 1984, Massone *et al.* 2006). Since then, researchers validated various fiber models for different structural components, boundary conditions and loading types. For instance, Petrangeli (1999b) developed and calibrated a fiber beam element with shear using test results of (1) short squat piers under constant axial loading, (2) RC beams with no web reinforcement and (3) rectangular column piers of a viaduct with insufficient longitudinal development length. Martinelli (2008) formulated a fiber element capable of accounting for cyclic nonlinear shear behavior and its coupling with bending based on the Moersch truss shear resisting mechanism. Model formulations were compared with short column tests under monotonic loading and cantilever specimens under cyclic loading. The model formulations yielded reasonable estimates of the experimental trends and indicated that opportunities for improvements exist in accurately capturing the initial stiffness and the collapse mechanism. Massone and Wallace (2004) contributed to the advancement of instrumentation layouts to experimentally separate the contribution of flexural and shear displacements utilizing experimental results obtained from slender walls tests by Thomsen and Wallace (2004). Their findings provided the basis and validation for a shear-flexure interaction model published by Massone *et al.* (2006). Massone (2010) extended the shear flexure interaction formulation to better predict the response of RC squat walls. Kolozvary (2014a, b) updated the model formulation by Massone *et al.* (2006) to account for cyclic loading effects by using test data from moderate aspect ratio RC shear walls published in Tran (2012). Ceresa *et al.* (2009) worked on a flexure-shear beam model to predict the cyclic response of RC beam-column members and RC shear walls subjected to axial force, flexure and shear. Particular attention was needed to accurately estimate the response for cracked cross sections. The research team observed good agreement between predictions and test data; nonetheless, limitations of the constitutive model and accurate estimations of the post peak strength degradation were identified as challenges.

While shear flexure interaction modeling has been extensively applied to superstructure elements as identified in the preceding literature review; foundation systems, such as Cast - In - Drilled - Holes (CIDH) shafts have been much less investigated due to the additional complexity of coupled nonlinear soil behavior contributing to the overall lateral pile response. CIDH shafts are very common reinforced concrete supporting elements for infrastructural systems (e.g., bridges) and urban commercial or residential constructions. During the design process, the expected load - deformation behavior of the pile foundation system is evaluated by modeling the pile structural properties, as well as the characteristics of the surrounding soil for a given pile material, pile geometry (diameter, depth), head boundary condition, and loading type. For good response

estimation it is necessary to accurately represent the interaction between the shaft and the soil by using a suitable modeling approach. Typically, nonlinear beam - column finite element models are used to evaluate the structural pile behavior, while the p - y approach is used to simulate the soil response. Hereby, p denotes the lateral resisting force of the soil and y represents the lateral pile/soil deflection. Most p - y formulations employed in current pile design date back to pioneering studies performed in the 1960s and 70s (Broms 1964a, b, Matlock 1970, Reese *et al.* 1975, O'Neill and Murchinson 1983, API 1987) and often yield pile-geometries that are uneconomical or unsafe. Uncertainties stem from limited test data for different head boundary conditions, pile geometries and materials, the use of constant or linear EI relationships and the site specific soil profiles.

Furthermore, the traditional derivation process of p - y formulations does not consider the impact of shear flexure interaction since typical pile instrumentation layouts consist of only pairs of longitudinal sensors (LVDTs and strain gauges attached to the longitudinal pile rebar). Therefore, the derived deformation profile is a result of flexural deformations alone (based on Bernoulli - Euler beam theory). Shear displacements however can contribute significantly to the overall pile response, in particular in fixed (rotation restrained) boundary regions, and reduce the overall load-displacement ductility. Fig. 1 shows schematically the deflection profile of a fixed head pile along with soil springs and indicates the regions where shear deformations could be expected.

In order to measure shear deformations experimentally, prior studies (Ahlberg 2008, Lemnitzer *et al.* 2010) have shown that a more comprehensive sensor layout; i.e., diagonal sensors along with longitudinal sensors, is needed to capture and separate deformations resulting from flexure and shear. Given the limited availability of such test data, the contribution of shear deformations to the overall response of an RC pile may be assessed with a structural model in the meanwhile. Hereby, an analytically obtained pile response using a model that considers only flexural deformations can be compared with in-situ test data and good agreement between an analytical model that considers "flexure-only" (Bernoulli-Euler beam theory) and test results would imply that shear deformations have no contribution to the overall pile response. In this case, current formulations would not

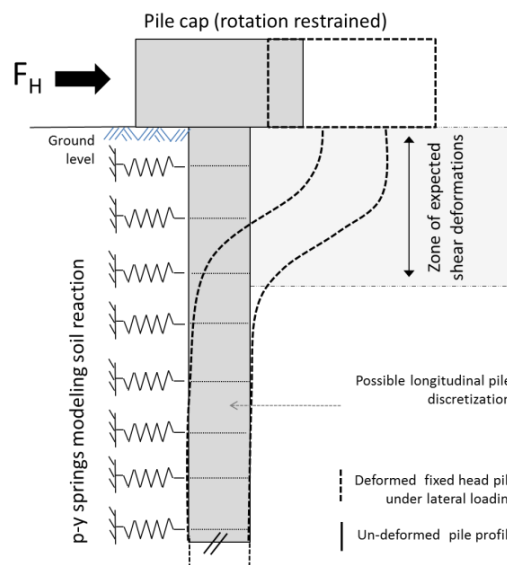


Fig. 1 Fixed head pile under lateral loading F_H

require adjustment for pile shear deformations. Contrary, when using an analytical model that captures shear-flexure interaction, differences between analytical and experimental results may hint to the contribution of structural shear and suggest a possible consideration of shear in the lateral response of pile foundations.

2. Objective

The primary objective of this paper is to use a shear flexure interaction model originally developed by Massone *et al.* (2006) for RC shear walls and assess its applicability to circular cross-sections. After a brief introduction of the model formulation, the authors present a verification study in which the model was applied to several column studies (i.e., without surrounding soil) to evaluate its numerical capabilities in capturing the structural pile/column response only. For brevity, this study is presented as statistical analysis. Once the suitability of the model for circular cross-sections can be verified, the authors apply this analytical tool to a fixed head pile foundation to assess the potential impact of nonlinear shear deformations on p - y curves by assessing the relative contribution of shear and flexure deformations to pile displacement and force profiles over the pile height. For comparison purposes, analytical modeling is once executed with a flexure-only model (Bernoulli-Euler beam theory) and again performed with a coupled shear- flexure analysis to highlight the important difference in the analytical approach.

3. Model description

The analytical studies were performed using the finite element program OpenSees (<http://peer.berkeley.edu/OpenSeesNavigator/>) provided by the Pacific Earthquake Engineering Research (PEER) center.

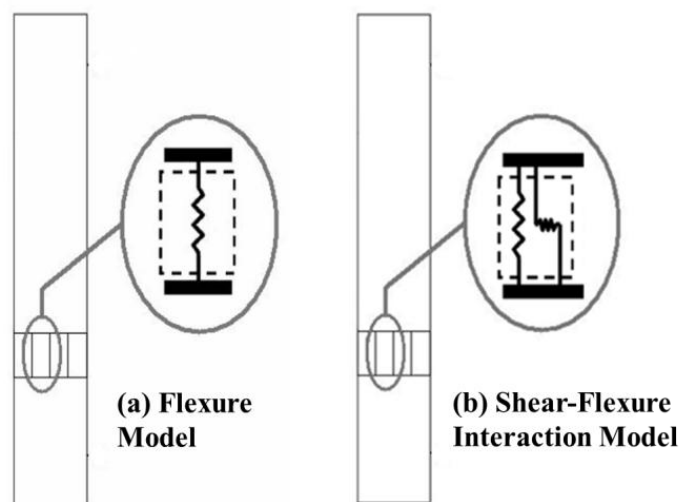


Fig. 2 Column discretization

3.1 Flexure model

The flexure model follows the simple process of nonlinear beam analysis. In this model, the structural element (wall, column or pile) is divided into regular elements along its length that are connected through nodes (Figs. 1 and 2(a)). Each element is sub-divided in a predetermined number of fibers (in the transverse direction) which are represented by a single spring with uniaxial behavior (Fig. 2(a)). In a bi-dimensional analysis, each element has three degrees of freedom per node (two displacements and one rotation), which are associated to strains via interpolation functions and the Bernoulli-Euler hypothesis (plane sections remain plane after loading). The flexure model follows similar principles as the shear-flexure interaction model described below, but only uses the uniaxial behavior of concrete and steel in the longitudinal direction to characterize the response; hence only axial behavior in flexure is modeled.

3.2 Shear-flexure interaction model

The Shear Flexure Interaction Model corresponds to a macroscopic biaxial fiber model that couples the axial and bending behavior with the shear behavior of a reinforced concrete (RC) element. Originally implemented into Opensees by Massone *et al.* (2006), the model couples shear and flexural responses of wall elements, and can be extended to beams and columns. Similar work was done for relatively slender elements by Petrangeli *et al.* (1999a) and validated for circular columns by Petrangeli *et al.* (1999b). The current model is a modification to the Petrangeli (1999b) model in that it also implements calibrated horizontal strain formulations (Massone *et al.* 2009, Massone 2010). The Massone *et al.* (2006) model considers every fiber to have a panel behavior, i.e., to have axial strains and also angular distortions in the plane of the element. This is an extension of the flexure model, by adding an additional lateral spring to the fiber, as shown in Fig. 2(b). Other models have used multifiber formulations to account for shear, such as the Timoshenko approach (Guedes *et al.* 1994, Mazars *et al.* 2006). The constitutive law is based on damage mechanics with parameters that account for shear. In the current formulation, shear is derived after applying equilibrium or providing a normal strain estimate in the transverse direction using a bi-axial constitutive law that accounts for concrete acting in the principal directions and steel in their longitudinal directions.

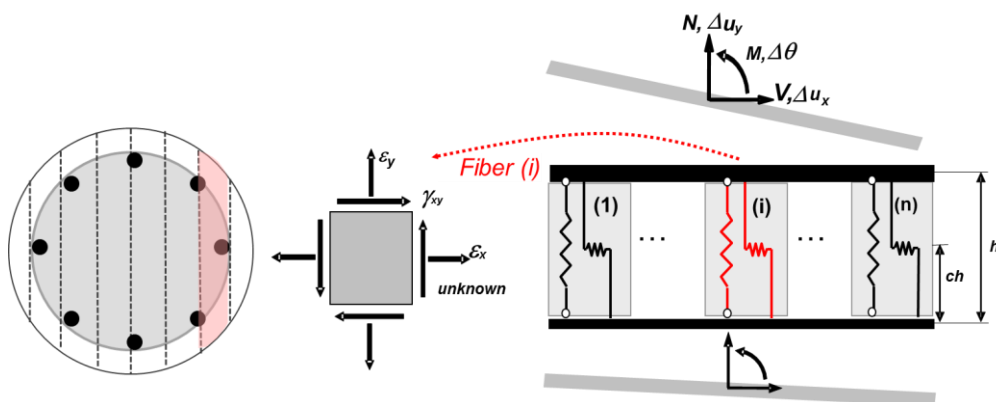


Fig. 3 Shear-Flexure interaction element (After Massone *et al.* 2006)

In longitudinal direction the column is divided into elements of defined length. In transverse direction, the cross-section is divided into fibers with panel behavior. In the interaction model, it is assumed that rotations are concentrated around a single point (center of rotation is assumed at the bottom of the element) and therefore located at a distance $c \times h$, where h is the total length of the fiber element and c is a constant less than 1. Previous works (Massone *et al.* 2006) have used values of $c=0.4$ to capture the linear curvature distribution of cantilever elements, however, well discretized elements have shown to have a good response estimation for values of $c=0.5$ (Massone *et al.* 2013, Kang *et al.* 2012), which is used in the analysis. Each element possesses six degrees of freedom, namely two displacements and one rotation at both ends of the element as shown in Fig. 3. Assuming that plane sections remain plane after deformation, and that the shear strain is uniform along the entire section, the angular distortion γ_{xy} and the longitudinal axial strain ε_y are calculated for all strips, based on the prescribed degrees of freedom for the current analysis step. Accordingly, each strip has two input variables ε_y and γ_{xy} , based on the element deformations. The transverse strain ε_x is initially estimated in order to complete the definition of the strain field. Then, by using the constitutive material relationships and the geometric properties, the stress field and forces can be determined. For calculating the unknown horizontal strain ε_x , two methods can be pursued. The first method assumes that the transverse axial stress is zero ($\sigma_x = 0$), which is consistent with the boundary conditions at the sides of the column with no transverse load applied over its height. Consequently, the value of ε_x is iterated until horizontal equilibrium is achieved. This method has shown good predictions when modeling slender walls, but discrepancies were observed when modeling walls with shear - span ratios less than 1.0 (Massone *et al.* 2006). In the case of piles, the lateral pressure applied by the soil might have an impact. However, this pressure is usually low compared to the concrete strength, and it is only applied to the side of the pile that reacts against the soil. For example, the pile considered in this analysis has a maximum lateral pressure of 1 MPa (zero on the other side) in a portion of the pile (which is not necessarily where the largest shear stress is observed), which in turn is only 2% of the confined concrete strength. Thus, the approach of $\sigma_x = 0$ is considered appropriate given the low lateral pressure. The second approach implements calibrated values of ε_x (received from experimental data or an analytical code) into the model, which has shown improvements on the prediction when modeling short walls (Massone *et al.* 2009, Massone 2010) and beams (Kang *et al.* 2012, Massone *et al.* 2013). This procedure does not require iterations.

3.3 Column discretization and material property formulations

Given the original development of the model for rectangular cross-sections, the column cross sections used in this verification study are transformed into equivalent rectangular sections, calculating the plain and confined concrete and reinforcement steel areas. A uniform strip width (d_w) was defined as $d_w = D/N$, where D is the column diameter and N is the prescribed number of strips or fibers (8 or 16 strips). Each fiber distinguishes between confined and unconfined concrete as shown in Fig. 4 and is defined through a coordinate location, a fiber area and the respective material properties. The longitudinal reinforcement area for each strip is calculated assuming that there is a uniform and continuous distribution in a circumference of diameter d . The reinforcement is modeled using the Menegotto-Pinto (1973) model, with initial and post-yield asymptotes selected to account for the effects of tension stiffening. This approach accounts for the softening (and weakening) of the average (smeared) stress-strain relationship of reinforcing bars embedded in concrete (due to concentration of strains in steel at crack locations) and was implemented in the

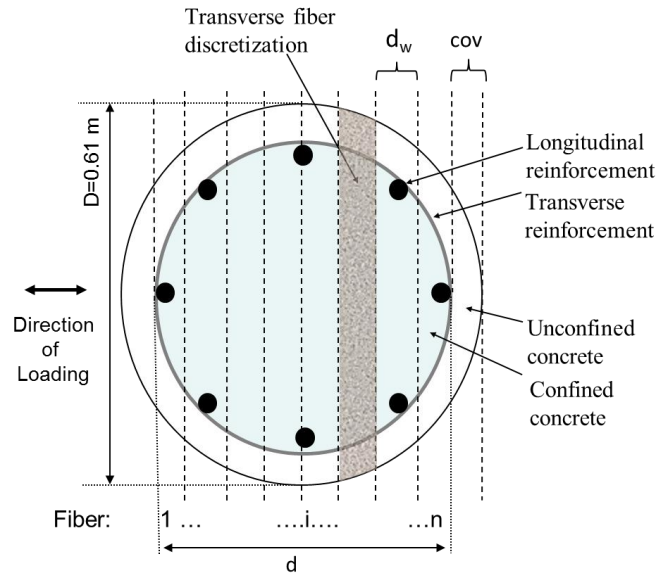


Fig. 4 Sample fiber discretization of column and pile cross sections (here: 10 fibers for demonstration only)

Menegotto-Pinto (1973) model using the relationships proposed by Belarbi and Hsu (1994).

The concrete was represented using a uniaxial material model. The confined concrete characteristics were determined using the Saatcioglu and Razvi (1992) relationship. The constitutive relationship employed in the analytical model for concrete considers the effects of biaxial compression softening (reduction in principal compressive stresses in concrete due to cracking under tensile strains in the orthogonal direction), and tension stiffening (average post-peak tensile stresses in concrete due to bonding of concrete and reinforcing steel between cracks). To incorporate the tension stiffening effect in the stress-strain behavior of concrete, the average (smeared) stress-strain relationship proposed by Belarbi and Hsu (1994) is implemented. To describe the stress-strain behavior of concrete in compression, the Thorenfeldt *et al.* (1987) based curve is used, as calibrated by Collins and Porasz (1989) and Carreira and Kuang-Han (1985), and updated via the introduction of the compression softening parameter proposed by Vecchio and Collins (1993). The described material models were used for both the flexural and the shear-flexure interaction models. The only difference is that the compression softening cannot be used in the flexural model.

4. Model verification - selected column studies

In order to assess the general applicability of the Massone *et al.* 2006 model and its capabilities of reasonably predicting the overall load deformation response of circular cross-sections, a total of ten experimental large scale column studies were selected for verification. Eight studies were chosen from the Pacific Earthquake Engineering Research (PEER, Berry *et al.* 2004) database and two additional column studies were taken from the Kawashima Earthquake Engineering Laboratory database of the Tokyo Institute of Technology (Kawashima Lab 2011). Both databases

Table 1 Column properties used in the verification analyses

Specimen		Failure Type	Geometry				Transverse Reinforcement		Longitudinal Reinforcement		Axial Load	Material Properties		
ID	REFERENCE		h_c [mm]	D [mm]	M/VD	D/ h_{st}	ρ_t [%]	Concrete Cover [mm]	Bar	ρ_l [%]		N/ $f_c A_g$ [%]	f'_c [MPa]	f_{yt} [MPa]
SPEC 1	Benzoni and Priestley (1994), S1	Flexure - Shear	914.5	610	1.5	5.3	0.28	15.9	12 $\phi 12.7$	0.52	5.7	30	361	462
SPEC 2	Benzoni and Priestley (1994), S2	Flexure - Shear	914.5	610	1.5	5.3	0.17	15.9	24 $\phi 12.7$	1.04	5.7	30	361	462
SPEC 3	McDaniel (1997), S1	Shear	1219.2	609.6	2	4.0	0.13	18.6	20 $\phi 15.9$	1.36	0.2	29.8	200	454
SPEC 4	McDaniel (1997), S1-2	Shear	1219.2	609.6	2	4.0	0.13	18.6	21 $\phi 15.9$	1.36	0.2	26.8	200	454
SPEC 5	McDaniel (1997), S2	Shear	1219.2	609.6	2	4.0	0.13	18.6	21 $\phi 15.9$	1.36	0.2	31.2	200	437.6
SPEC 6	Petrovski and Ristic (1984), M2E1	Flexure - Shear	900	307	2.93	2.7	0.63	36	12 $\phi 12$	1.83	5.5	35.9	240	240
SPEC 7	Petrovski and Ristic (1984), M2E2	Flexure - Shear	895	307	2.92	2.7	0.63	36	12 $\phi 12$	1.83	10	34.4	240	240
SPEC 8	Wong <i>et al.</i> (1990), S2	Flexure - Shear	800	400	2	4.0	0.47	18	20 $\phi 16$	3.2	39	37	340	475
SPEC 9	Yoneda Kashima and Shoji - tp021	not - reported	1350	400	3.38	2.4	0.26	70	12 $\phi 16$	1.89	4.9	30	363	374
SPEC 10	Yoneda Kashima and Shoji - tp024	not - reported	1350	400	3.38	2.4	0.13	70	12 $\phi 16$	1.89	4.9	30	363	374

^[1] D/h_{st} ratio (column diameter to element height) for the model formulation with 8 elements along the column height.

^[2] ρ_t is the volumetric transverse reinforcement ratio, calculated as the volume of transverse reinforcement over the confined concrete volume. It is calculated as $\rho_t = 4A_s / sbc$, where A_s is the area of the hoop bar, s is the hoop vertical spacing and b_c is the confined area diameter, measured center to center of the hoop bar.

^[3] h_c element height

^[4] M/VD moment-to-shear length ratio

^[5] ρ_t, ρ_l transverse and longitudinal reinforcement ratio

^[6] f'_c, f_{yt}, f_{yl} concrete and steel (transverse and longitudinal) strength

provide material properties, specimen geometries, details on the experiment and the specimen's load-displacement response. Tests are separated in the database according to their failure types and test characteristics. The specimens were selected based on similarities with the pile foundation that will later be implemented into this study. Parameters included the column geometry, failure type and the observation of shear degradation in the load displacement response to validate the

Table 2 Summary of model configurations applied to each column specimen

Model	Transverse Discretization	Longitudinal Discretization	Stress & Strain Assumptions	Configuration #
Flexure Model	8 Fibers	8 Elements		1
		8 Elements		2
Shear-Flexure Interaction Model	8 Fibers	$\frac{D}{h_{st}} = 2$ - Elements	$\sigma_x = 0$, ε_x iterated	3
		8 Elements		4
	8 Elements	ε_x calibrated	5	
	16 Fibers	$\frac{D}{h_{st}} = 2$ - Elements	$\sigma_x = 0$, ε_x iterated	6
		8 Elements		7
		8 Elements	ε_x calibrated	8

*D=diameter of the pile

h_{st} =vertical element length (height)

capabilities of the shear-flexure interaction model to reproduce the test results. Table 1 shows the full information of all ten specimens. All tests were evaluated with the “flexure only” and with the “shear- flexure interaction” model, as explained above. Among the two different models, sub-configurations with varying transverse and longitudinal discretizations were selected as shown in Table 2. Transverse discretizations (Fig. 4) consisted of either 8 or 16 fibers, while longitudinal discretizations (Fig. 1) included constant length elements (8 elements) or multiple elements with consistent lengths (heights h_{st}) close to $D/2$. The selection of an element length of $D/2$ was found a suitable alternative for the numerical model given that shear cracks and concrete spalling along apparent compression struts were observed in the field within 1.5 pile diameters below ground surface (Lemnitzer *et al.* 2010).

The variation of the studies also included the model’s stress - strain assumptions (ε_x iterated or calibrated) as shown in Table 2. In the “calibrated model” ε_x was estimated using a general expression derived from a finite element formulation suggested by Massone *et al.* (2010). This code uses the specimen geometry, reinforcement ratios, boundary conditions, axial load, aspect ratio and drift level to provide “calibrated”, i.e., specimen specific estimations of the horizontal strain ε_x .

4.1 Analysis of the column response

The load - displacement responses obtained from the analyses are statistically compared with the test data by evaluating the maximum column capacity in shear (V), the column rigidity (K) at 60% of the ultimate capacity and the degradation displacement (D) at 10% of capacity loss. Figs. 5(a)-(c) show a comparison of the ratios of the component (capacity, stiffness or displacement) obtained from the flexure-only and shear-flexure-interaction analyses divided by the respective value measured in the experimental column study. Table 3 provides a tabulated overview of the results shown in Fig. 5 and includes the average value of the depicted ratios along with the standard deviation $\bar{\sigma}$ of the average.

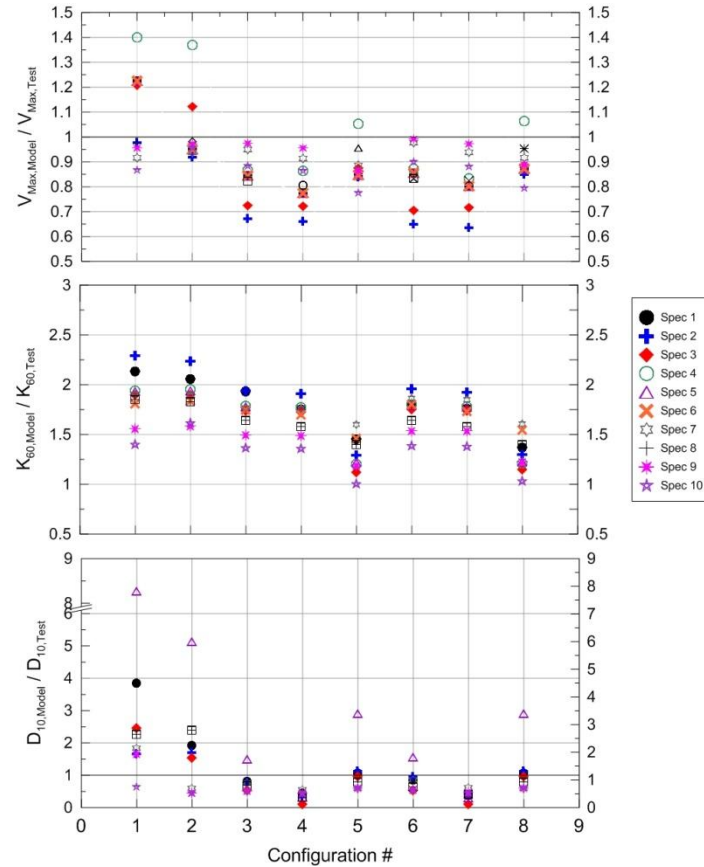


Fig. 5 Comparison of model vs. test results for the selected 10 column specimens

A comparison of the column capacities (Fig. 5, Table 3) indicates that the shear - flexure interaction model yields better results when using calibrated horizontal strain values ε_x , than the $\sigma = 0$ procedure. Using 16 fibers, the calibrated ε_x procedure yields an average capacity ratio \bar{v} of 0.91, which indicates a difference between the analytical and experimental results of only 9% (Configuration #8). The $\sigma = 0$ procedure yielded a mean value of 0.84 when 8 elements were used in the longitudinal direction, and 0.86 when the element number satisfied $D/h_{st}=2$ (Configuration 6 & 7). The flexural model yielded a mean maximum lateral load ratio \bar{v} of 1.00 and 1.10 for 8 and 16 fibers, respectively. However; the flexure model showed a higher dispersion of the data than any of the shear flexure interaction model formulations. The standard deviation $\bar{\sigma}$ for the flexure model was calculated to be $\bar{\sigma} = 0.19$, whereas the standard deviation for the shear flexure interaction model was about half, i.e., $\bar{\sigma} = 0.1$ for the $\sigma_x = 0$ procedure with 8 elements in the longitudinal direction; $\bar{\sigma} = 0.11$ for $\sigma_x = 0$ with a constant element discretization ratio $D/h_{st}=2$, and $\bar{\sigma} = 0.09$ for the procedure with the calibrated ε_x values.

To enable a better visualization of the model performance, a sample set of experimental load displacement relationships for column specimens 5, 7 and 8 is compared with various model configurations and presented in Figs. 6-8. The Figures show results for the 16 fiber configurations 7, 8 and 9 from Table 2 which are almost identical to the 8 fiber configurations 4, 5 and 6 (see Fig.

5); hence only one set is shown in Figs. 6-8. For each specimen, test data are compared to the flexure-only model (Configuration 1) as well as with the shear-flexure interaction (S-F) models (Configurations 7-9). Fig. 6 depicts the load displacement relationship for Specimen 5, which is a column specimen that experimentally failed in shear (see Table 1). Test results are reasonably well captured by all shear-flexure interaction models in terms of maximum capacity and onset of strength degradation. The flexure only model shows a much higher ductility than the test results as shown by the steadily increasing load capacity. Specimen 7 (Fig. 7) represents an example of a relatively slender specimen with low longitudinal reinforcement. As this specimen is more prone to flexural failure, all models perform relatively similar. Specimen 8 (Fig. 8) failed in shear-flexure

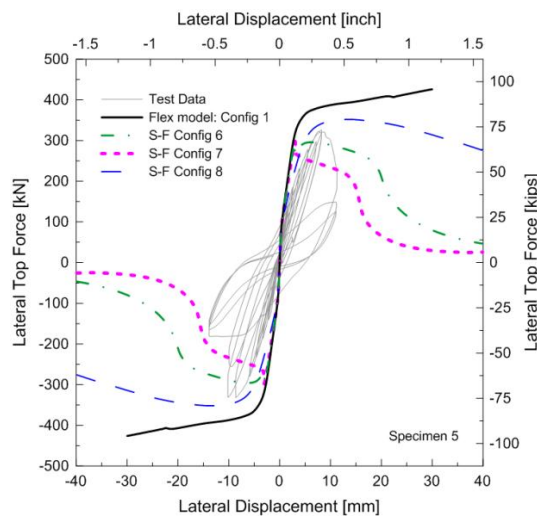


Fig. 6 Load displacement comparison between test data and model configurations 6,7 and 8 for Specimen 5 (shear failure)

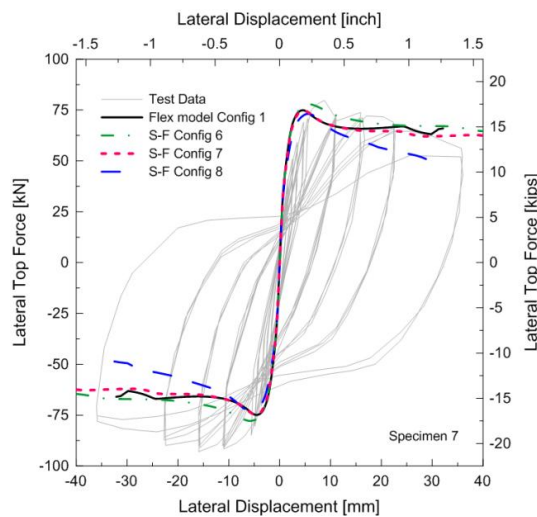


Fig. 7 Load displacement comparison between test data and model configurations 6,7 and 8 for Specimen 7 (flexural failure)

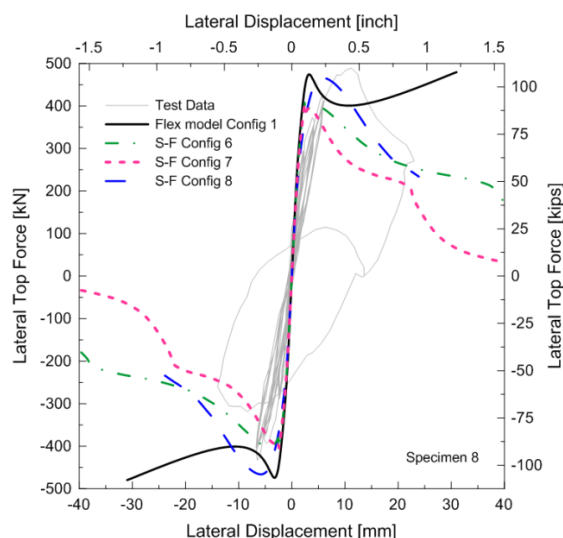


Fig. 8 Load displacement comparison between test data and model configurations 6,7 and 8 for Specimen 8 (shear-flexural failure)

interaction. The flexural model shows more ductile response after some minor degradation which is likely associated with the loss of concrete cover. This specimen was subject to high axial loading and the ductility can be attributed to the amount of longitudinal steel in the specimen. The overall load displacement relationship is best captured with S-F configurations 6 and 8. Similarly to Specimen 5, the flexural model cannot capture any strength degradation shown by the steady increase in load vs. displacement.

The rigidity of the column at 60% of its maximum capacity was evaluated in a similar fashion as the maximum strength, namely, by calculating the ratio of the secant rigidity at 60% of maximum lateral load obtained from the analysis, labeled $K_{60,Model}$, over the secant rigidity at 60% of maximum lateral load of the test, labeled $K_{60,Test}$. The 60% value was deemed appropriate as it describes the stiffness after crack initiation and prior to specimen yielding. ASCE/SEI 41-06 Chapter 3 (2007) [formerly FEMA 356] uses a similar recommendation, but implements 60% K_{yield} rather than 60% of the stiffness adjusted to the max capacity value. Table 3 shows the stiffness ratios for all 8 analysis configurations. Fig. 5(b) depicts the comparison of all analytical runs for all 10 columns. Results indicate that a much closer prediction of the stiffness was achieved with the shear flexure interaction model. Again the calibrated model provided the closest stiffness estimation ($\bar{K}_{60}=1.3$), while the $\sigma_x=0$ models over-predicted the stiffness by more than 50% ($\bar{K}_{60}=1.7$). Results were identical for the use of 8 or 16 fibers in transverse discretization. The flexure-only model was not found suitable to provide acceptable estimates of the column stiffness. A stiffness close to twice as measured ($\bar{K}_{60}=1.9$) was obtained with the flexure only model.

The mean displacement at 10% of capacity loss, \bar{D}_{10} , was obtained from the analysis $D_{10,Model}$ over the same parameter obtained from the test ($D_{10,Test}$). As the flexure-only model by definition does not incorporate shear degradation, the values observed in the analysis yield expectedly high values. The shear-flexure-interaction models with 8 elements in the longitudinal direction using iterated strain formulations ε_x showed a very fast degradation in the column response due to damage localization, producing average values of \bar{D}_{10} of 0.44 and 0.42. Hence this configuration

Table 3 Results of the column study

Model	Transverse Discretization	Longitudinal Discretization	Model Config #	$\hat{V} = \frac{V_{Max,Model}}{V_{Max,Test}}$	$\bar{\sigma}(\hat{V})$	$\hat{K}_{60} = \frac{K_{60,Model}}{K_{60,Test}}$	$\bar{\sigma}(\hat{K}_{60})$	$\hat{D}_{10} = \frac{D_{10,Model}}{D_{10,Test}}$	$\bar{\sigma}(\hat{D}_{10})$	
Flexure Model	8 Fibers	8 Elements	1	1.1	0.24	1.9	0.25	3	2.4	
	16 Fibers	8 Elements	2	1	0.19	1.9	0.19	2	1.9	
Shear Flexure Interaction Model	8 Fibers	D/h _{st} =2 Elements	$\sigma_x=0, \epsilon_x$ iter	3	0.85	0.09	1.7	0.18	0.83	0.37
		8 Elements	$\sigma_x=0, \epsilon_x$ iter	4	0.83	0.09	1.7	0.16	0.44	0.22
	16 Fibers	8 Elements	ϵ_x cali	5	0.9	0.10	1.3	0.18	1.2	0.92
		D/h _{st} =2 Elements	$\sigma_x=0, \epsilon_x$ iter	6	0.86	0.11	1.7	0.17	0.86	0.38
		8 Elements	$\sigma_x=0, \epsilon_x$ iter	7	0.84	0.10	1.7	0.16	0.42	0.15
		8 Elements	ϵ_x cali	8	0.91	0.09	1.3	0.18	1.2	0.92

is somewhat unsuitable for the planned study. The same procedure with calibrated strain values yielded a closer estimation of the measured post peak displacement ($\hat{D}_{10}=1.2$) but generated very high average standard deviations ($\bar{\sigma}=0.92$). A much better overall estimation was obtained with the shear flexure interaction model using D/h_{st}=2 number of elements in the longitudinal direction. Average displacement ratios \hat{D}_{10} of 0.83 and 0.86 were obtained with standard deviations of only 0.22 and 0.15 for 8 and 16 fibers, respectively.

In summary, all models showed good prediction of strength with relatively little variation in the analyses. Results of the shear flexure interaction model were within 10% of the measured results which indicates a good predictability of the ultimate capacity. Most models overestimated the actual specimen stiffness. The closest predictions could be obtained with calibrated ϵ_x formulations. The displacement response varied throughout the different configurations. The flexure model does not show degradation and can be excluded from further consideration. A longitudinal discretization of D/h_{st}=2 elements provided the overall best combination of closely prediction the displacement with a reasonable standard deviation of the results. Since post peak capacity degradation is an important issue in modeling, this configuration will be used for the following pile analyses. Discretization of 8 and 16 fibers showed similar results; hence no significant improvement was obtained by refining the cross-section discretization. Additional sensitivity studies with varying transverse reinforcement and concrete confinement was performed outside the presented material. Minimal influence of the two parameters was observed. Therefore, configuration 3 in Table 3 will be selected for the consecutive studies.

5. Application of the model to a 0.61m fixed-head pile foundation

The experimental study selected for comparison with the proposed analysis was part of a comprehensive large scale testing program of bridge foundation systems performed between 2000 and 2006 at the University of California, Los Angeles and funded by the California Department of Transportation (CALTRANS). The specific test specimen, a 0.61 m diameter, fixed head,

reinforced concrete CIDH shaft is extensively described in Stewart *et al.* (2007), Lemmitzer *et al.* (2010) and Khalili-Tehrani *et al.* (2014). The pile is depicted in Fig. 9 which shows a photograph of the pile reinforcement (Fig. 9(a)) and the pile cap at the construction site immediately before testing (Fig. 9(b)). More details on the test specimen, experimental test results and photo documentation can be found on the NEES project warehouse under Lemmitzer *et al.* (2014).

The total length of the pile was 7.5 m below ground surface (experiment and model). The vertical model discretization is shown in Fig. 10. The pile is modeled using 25 elements ($D/h_{st}=2$) with an element size of $h_{st}=30$ cm, based on the outcomes of the verification study presented above. A single, rigid element, 91 cm long, is used above ground-line to allow the lateral load or displacement to be applied at a location consistent with the test condition (pile cap). The top node is restrained against rotation, but allowed to translate laterally. Vertical displacement at the top of the pile was unrestrained. The shaft was designed using a 28 MPa concrete mix, however, cylinder tests gave values of f'_c between 30 and 36 MPa. Therefore, in the analytical model, unconfined concrete areas were assigned an average compressive strength f'_c of 32 MPa at a concrete strain ε_c of 0.0023. The confined concrete characteristics were determined using the Saatcioglu and Razvi (1992) relationship, resulting in a confined compressive strength $f'_{cc}=51$ MPa at concrete strain $\varepsilon_{cc}=0.0089$.

The clear concrete cover was 6 cm. The longitudinal reinforcement in the field consisted of 8 #9 bars ($d_b=29$ mm) A706, Grade 60 steel, with a measured yield stress of 483 MPa. Transverse reinforcement consisted of 48 cm diameter spirals made of #5 bars ($d_b=16$ mm) spaced at 11 cm pitch over the length of the pile. In the shear-flexure-interaction model, the reduced (or softened) yield stress for the longitudinal reinforcement was taken as 439 MPa, with a post yield strain hardening ratio of $b=0.008$, with b describing the ratio between initial and post yield stiffness. The material properties for the transverse reinforcement were assumed to be identical to those of the longitudinal reinforcement.

The soil is represented using a series of nonlinear springs attached to the nodes of the pile elements and is described mathematically using a tri-linear fit of the fixed head p - y curves specifically derived for this pile and soil configuration by Khalili-Tehrani *et al.* (2014). Hereby, we are removing any bias that might be introduced by using generic API p - y relations, and only

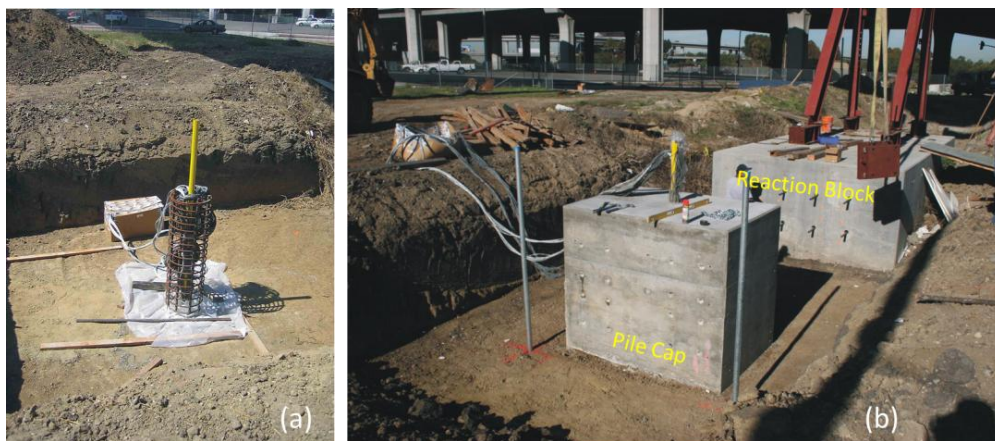


Fig. 9 Photograph of Fixed Head Pile during Construction (a) Reinforcement Cage, (b) Pile Cap and Reaction Block (Photo Credit: E. Ahlberg)

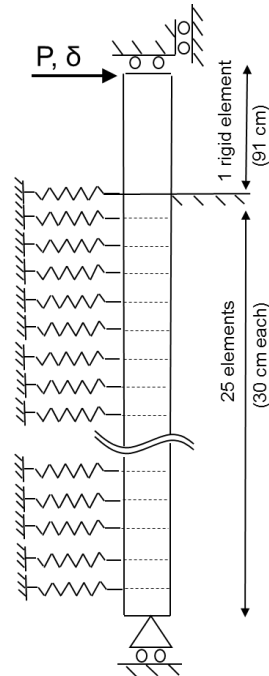


Fig. 10 Model discretization for fixed-head pile

assessing the potential impact of nonlinear shear deformations.

Given the scatter in experimental curvature data obtained from instrumentation such as strain gauges, LVDTs, inclinometers and fiber optic sensors, a traditional double derivation and integration process was not able to provide reliable p - y curves from test data. Therefore, the research group (see Khalili-Tehrani *et al.* 2014) developed an alternative approach using the FrameLab model (Tacioglu *et al.* 2006) to derive the p - y curves for the fixed head pile. This model is based on Bernoulli Euler beam theory, that is, plane sections are assumed to remain plane after loading and uniaxial material models are used for longitudinal reinforcement, cover (unconfined) concrete, and confined (core) concrete. The functional form of the p - y curve was assumed to match that used by API (1993), except with undetermined coefficients, and the error was minimized in a least-squares sense between the measured top load vs. top displacement relationship and the top load vs. top displacement relation predicted using a pile model that considers only flexural behavior with appropriate boundary conditions. A detailed explanation of the process used is also presented in Stewart *et al.* (2007). Interaction between nonlinear axial-bending and shear behavior is consequently not considered in that model. Therefore, if significant shear-flexure interaction exists, the fitting procedure via the “flexure only” Frame Lab model used to determine the p - y relations may substantially underestimate structural shear deformations, and the derived p - y relations account incorrectly for this added shear-flexibility. A difference in the overall load displacement curve should therefore be noticeable when comparing the experimental data with the Massone *et al.* shear-flexure-interaction model. A good agreement shall be expected between the test data and the flexure-only model when using the Khalili-Tehrani *et al.* p - y curves.

In the Open Sees Model, fixed boundaries were assigned to end nodes of the soil springs letting the pile move relatively to the soil. Other studies found in literature have incorporated the soil-

structure interaction as a macro model, combining or condensing the pile and soil behavior (Correia *et al.* 2012) or have studied the pile response under a 3D finite element simulation including the surrounding soil (Li *et al.* 2014). Since the focus of our work is to provide insight into the possible impact of the shear component in the p - y derivation process, the traditional p - y approach has been chosen as SSI representation in our model.

5.1 Model results

5.1.1 Pile head load-displacement relationships

The fixed head shaft lateral load versus lateral top displacement response is shown in Fig. 11. The “flexure” model matches the experimental results with respect to initial stiffness well and captures the maximum lateral experimental force of about 1214 kN at a displacement of 5 cm. This match was expected, as the p - y relations were derived without the consideration of potential shear deformations, and were fitted to match the overall pile head displacement response. Unfortunately no strength degradation over the tested displacement range was obtained with the flexure-only model, which introduces a severe error when comparing model and test data and implies that the initiation of pile failure is a result of a shear-flexure mechanism. The maximum lateral load for the coupled shear-flexure interaction model is only 1110 kN, or approximately 10% less than the “flexure-only” model. The lateral strength is achieved at a lateral displacement of approximately 10 cm, and lateral strength degradation (pile failure) is observed for the shear-flexure interaction model at a lateral displacement of 11.5 cm; lateral strength degradation is observed in the test results at approximately 7.5 cm.

In Fig. 11, the behavior at loads less than about 700 kN is essentially the same for the two models. Since the same p - y relations were used for both cases, if the coupled model reasonable represents the nonlinear behavior of the reinforced concrete pile, which is expected, results imply that p - y curves derived by Khalili-Tehrani *et al.* (2014) could be too soft. To derive consistent relations, use of a coupled model is required during the p - y back-calculation procedure. Fig. 11

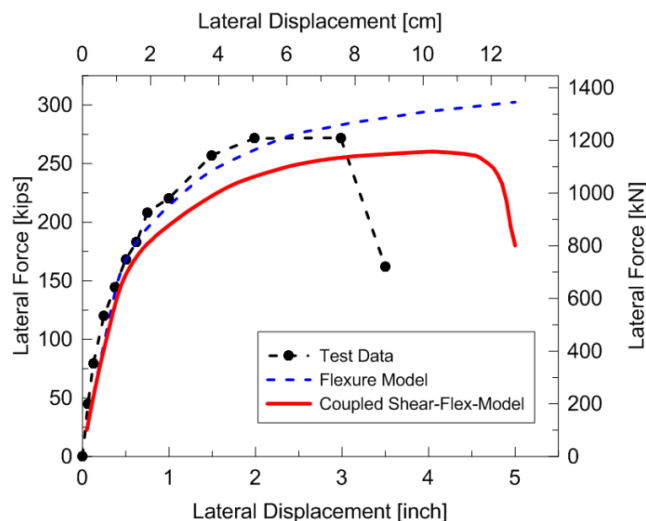


Fig. 11 Load-displacement response of fixed head pile using the “flexure-only” and “shear-flexure interaction model”

indicates schematically the shift of the model load-displacement curve when using p - y curves that accurately account for this effect. A re-calibration of the implemented p - y formulations is suggested and would likely also capture the point of capacity degradation better.

5.1.2 Lateral pile displacement profiles

The flexural, shear and total lateral pile displacements along the pile were obtained at various lateral top displacement levels using the shear-flexure interaction model (Fig. 12). Shear deformations were acquired directly from the analytical model and flexural deformations were calculated by subtracting the shear contribution from the total pile deformation. Shear displacements (Fig. 12(b)) in the fixed head pile contribute up to 40% to the total pile lateral displacements and are concentrated right below ground line (up to about 60 cm depth). Other locations show nearly zero shear displacement. Parametric studies not presented in this manuscript showed that smaller longitudinal pile discretizations showed similar concentration of shear deformations at the pile top; hence the chosen discretization did not influence the overall pile response. Flexural deformations are observed between ground line and a pile depth of 240 cm (~4d), and account for up to 60% to the total displacements. At lateral top displacements exceeding approximately 5 cm, flexural displacements increase by only small increments (Fig. 12(a)) while shear displacements become large, indicating that the loss of lateral strength is associated with shear failure.

5.1.3 Moment profiles

The fixed head pile moments (Fig. 13) indicate that yielding occurs in two locations, just below the pile cap in negative bending and roughly at 200 cm (~3d) below ground line in positive bending. Bending moments approach zero at depths below 500 cm. Based on a section analysis

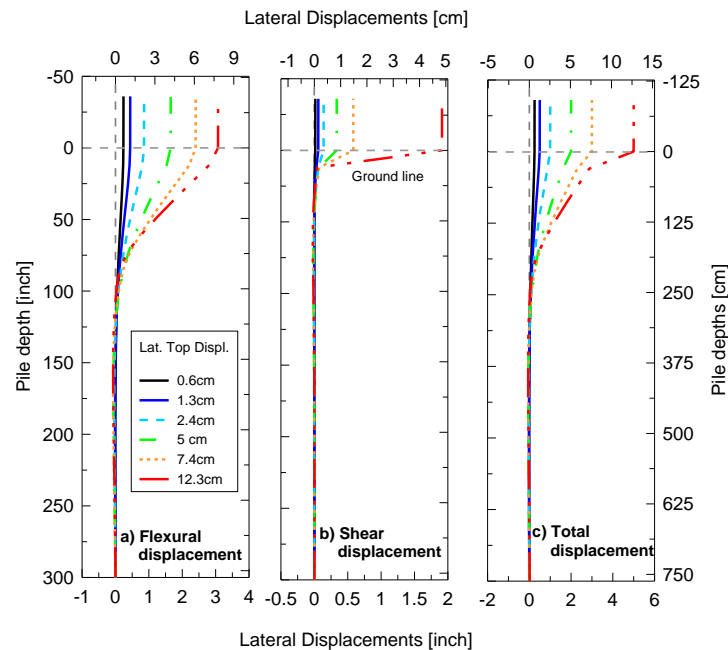


Fig. 12 Displacement profiles for the fixed head shaft

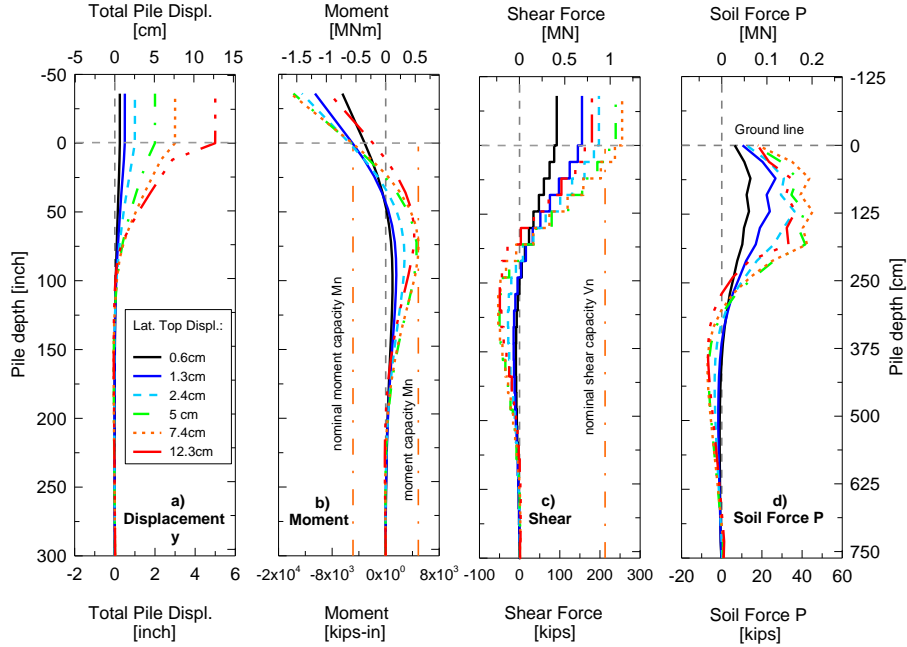


Fig. 13 Displacement, moment, shear and soil reaction profiles for fixed head pile

using in-situ shaft properties, the yield (M_y) and nominal (M_n) moments were computed as 450 and 565 kN-m, respectively, which are plotted on Fig. 13(b) as vertical lines. Initial pile yielding was reached just below ground line at a lateral top displacement of 1.3 cm and the nominal moment capacity was achieved at a lateral top displacement of 2.4 cm. The second plastic hinge at a depth of 3d formed at a lateral displacement of 4 cm (point of yielding) and the nominal capacity was reached at the same depth at a lateral top displacement of 5 cm.

5.1.4 Shear profiles

The fixed head pile shear forces range between 1130 kN at the top (maximum applied force) and -240 kN at a pile depth of 300 cm (~5d). The nominal shear capacity (V_n) of the fixed head shaft was calculated using the ATC-32 (1996) recommendations for circular cross-sections as

$$V_s = \frac{\pi A_{sp} f_{yh} D'}{2s} \quad (1)$$

$$V_c = 0.166 \sqrt{f'_c} A_e \quad (2)$$

$$V_n = V_s + V_c \quad (3)$$

where D' is the diameter of the hoop reinforcement measured to the hoop centerline (50.8 cm), s is the vertical hoops spacing (11.4 cm), f_{yh} is the yield strength of the hoops (483 MN/m²), A_{sp} is cross-sectional area of the hoop (2 cm²), A_e is the effective shear area of the shaft (2918.6 cm²) and f'_c is the concrete compressive strength 32.4 MPa. V_s denotes the shear strength due to transverse reinforcement, V_c represents the concrete shear strength and V_n is the nominal shear strength of the

section. Plugging these values into Eqs. (1)-(3), yields shear strengths of $V_s=674$ kN, $V_c=276$ kN and $V_n=950$ kN. Shear forces reached their nominal shear strength at the pile-cap interface. The analytical results are consistent with test observations which revealed relatively large diagonal cracks at the pile-cap interface along with spalling of concrete along the diagonal compressive struts for the tests performed on piles with fixed head boundary conditions.

Pile moment and shear profiles are compared in Fig. 14 for the flexure-only model and the coupled model, using a lateral displacement level of 7.4 cm and 12.3 cm. It can be seen that use of the coupled model does not impact the moment and shear profiles significantly at smaller displacements and that the primary impact is on lateral displacements (Fig. 12). However, once shear failure initiates (as degradation in Fig. 11), more significant differences between model results (flexure, versus shear-flexure) are observed in the moment and shear profiles.

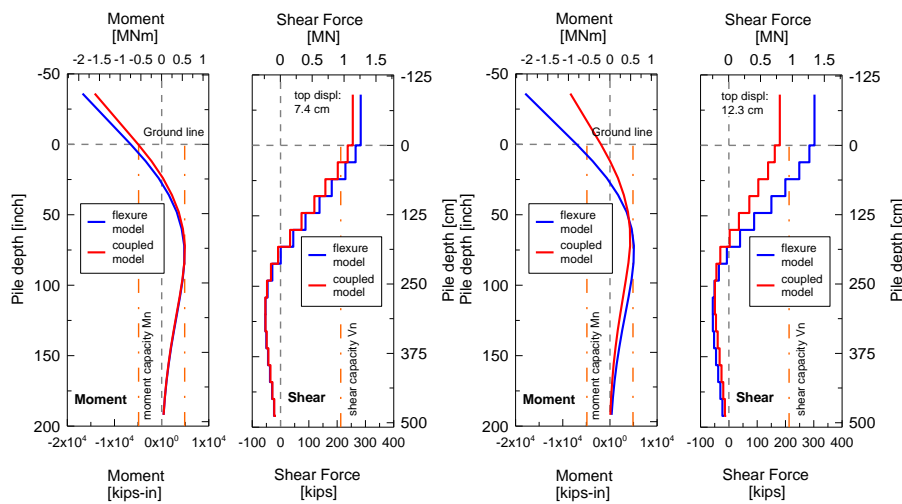


Fig. 14 Comparisons of moment and shear forces for the fixed head pile at lateral top displacements of 7.4 and 12.3 cm

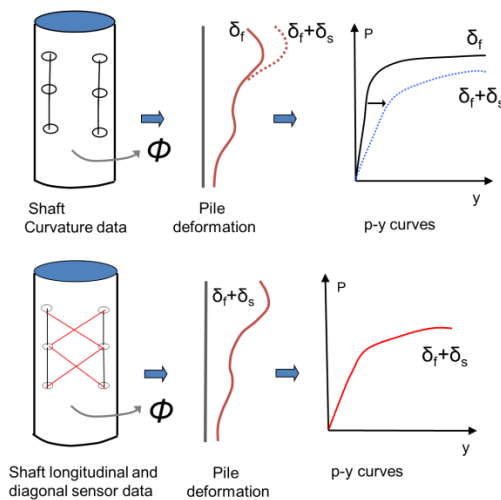


Fig. 15 Proposed Instrumentation and p - y derivation

6. Conclusions

The analytical shear-flexure interaction model confirmed the anticipated contribution of shear deformations to the overall lateral pile response. Despite these promising comparisons, the authors recognize that great potential for more complex sensitivity studies exists. A general comparison of the impact of shear flexure interaction on the pile response shows that differences observed in moment and shear forces between the flexure and the coupled shear flexure interaction model are rather small compared to the impact that the shear flexure interaction has on the pile displacements profile. Instrumentation layouts capturing shear deformations based on diagonal sensor installation as proposed for reinforced concrete walls (Massone *et al.* 2006) and executed by Stewart *et al.* (2007) are suggested for future studies on reinforced concrete piles to account for the effect of shear deformations in fixed head piles. Fig. 15 shows schematically how consideration of flexure and shear deformations results in larger total pile deformations, and produces a softer p - y curve (i.e., larger soil displacements at a given force level) when using the traditional p - y derivation process (i.e., via curvature double integration and derivation).

7. Summary and recommendations

A shear-flexure interaction model, originally developed for RC shear walls by Massone *et al.* (2006), and implemented in the open source software OpenSees, was modified and applied to a series of experimental column studies to investigate its ability to reasonably predict the structural response of circular cross-sections under lateral loading. Model parameter variations included the longitudinal and transverse discretization and the stress-strain assumptions. Most accurate response estimation was found for a model formulation with a discretization of 8 fibers in transverse direction and 25 elements in longitudinal direction with an element length of $D/h_{st}=2$. The model was then applied to a 0.61 m diameter RC pile foundation to identify if structural shear deformations impact the lateral pile response and needed to be accounted for when deriving p - y formulations typically used to represent the soil response during pile design.

The pile configuration and material parameters used in this study were calibrated to match those used in the experimental study of large scale pile foundation systems conducted by Stewart *et al.* (2007). In this study, the 7.5 m deep reinforced concrete shaft had longitudinal reinforcement consisting of 8 # 9 bars and spiral transverse reinforcement consisting of 16 mm nominal diameter bars with a vertical pitch of 11.4 cm.

The soil is modeled using pile specific p - y curves for the fixed head boundary condition derived by Khalili-Tehrani *et al.* (2014). Results indicate that shear deformations significantly influence the overall top load displacement response for displacements exceeding 0.6 cm, even though the shear force in the pile does not reach the nominal pile shear capacity until a lateral displacement of 5.0 cm. Shear deformations along the pile depth for the coupled model were found to account for up to 40% of the total lateral displacement and reached their maximum contribution (analytically) where significant lateral strength degradation was observed experimentally, hence providing a good correlation between in-situ pile behavior and model findings. The shear-flexure interaction model underestimates the lateral top load at lateral displacements exceeding 2.5 cm by approximately 10% because the p - y curves used in this study were calibrated to provide a good fit for a flexure-only model. The results suggest that the actual p - y curves are stiffer than those derived by Tehrani *et al.* (2014). A future publication, currently in preparation, targets the re-

calibration of the utilized p - y formulation to account for structural shear flexure interaction and suggest the implementation of a softening parameter in the hinge region to indirectly implement the additional deformation currently not considered in commonly used lateral pile design methods, i.e., p - y formulations.

References

- Ahlberg, E.R. (2008), "Interaction between soil and full-scale drilled shaft under cyclic lateral loads", Ph.D. Dissertation, University of California, Los Angeles, CA.
- American Petroleum Institute (API) (1987), "Recommended practice for planning, designing, and constructing fixed offshore platforms", *API Recommended Practice 2A (RP-2A)*, 17th edn.
- ASCE/SEI 41-06 (2007), "Seismic Rehabilitation of Existing Buildings", American Society Of Civil Engineers, Reston.
- Belarbi, H. and Hsu, T.C.C. (1994), "Constitutive laws of concrete in tension and reinforcing bars stiffened by concrete", *ACI Struct. J.*, **91**(4), 465-474.
- Berry, M., Parrish, M. and Eberhard, M. (2004), PEER Structural Performance Database User's Manual (Version 1.0). Pacific Earthquake Engineering Research Center, University of CA, Berkeley, http://nisee.berkeley.edu/spd/performance_database_manual_1-0.pdf.
- Broms, B. (1964a), "Lateral resistance of piles in cohesionless soils", *J. Soil Mech. Found. Div.*, **90**(3), 123-156.
- Broms, B. (1964b), "Lateral resistance of piles in cohesive soils", *J. Soil Mech. Found. Div.*, **90**(2), 27-63.
- Carreira, D.J. and Kuang-Han, C. (1985), "Stress-strain relationship for plain concrete in compression", *ACI Struct. J.*, **82**(6), 797-804.
- Ceresa, P., Petrini, L., Pinho, R. and Sousa, R. (2009), "A fibre flexure-shear model for seismic analysis of RF-framed structures", *Earthq. Eng. Struct. Dyn.*, **38**(5), 565-586.
- Chan, E.C. (1982), "Nonlinear geometric, material and time-dependent analysis of reinforced concrete shells with edge beams", Ph.D. Dissertation, University of California, Berkeley, Berkeley.
- Collins, M.P. and Porasz, A. (1989), "Shear strength for high strength concrete", *Bull. No. 193 - Design Aspects of High Strength Concrete*, Comite Euro-International du Beton (CEB), 75-83.
- Correia, A.A., Pecker, A., Kramer, S.L. and Pinho, R. (2012), "Nonlinear Pile-Head Macro-Element Model: SSI effects on the Seismic Response of a Monoshaft-Supported Bridge", *Proceedings of the 15th World Conference on Earthquake Engineering*, Lisbon, Portugal.
- Guedes, J., Pegon, P. and Pinto, A.V. (1994), "A Fibre/Timoshenko Beam Element in CASTEM 2000", In *Special Publication Nr. I.94.31*, Italy: Applied Mechanics Unit, Safety Technology Institute, Commission of the European Communities, Joint Research Centre, Ispra Establishment.
- Kaba, S.A. and Mahin, S.A. (1984), "Refined modelling of reinforced concrete columns for seismic analysis", *Technical Report UCB/EERC-84/03*, University of California, Berkeley, Berkeley, CA.
- Kang, T.H.-K., Kim, W., Massone, L.M. and Galleguillos, T.A. (2012), "Shear-flexure coupling behavior of steel fiber-reinforced concrete beams", *ACI Struct. J.*, **109**(4), 435-444.
- Kawashima Research Group (2011), Database with the results of cyclic lateral - load tests of reinforced concrete columns, <http://seismic.cv.titech.ac.jp/>.
- Khalili-Tehrani, P., Ahlberg, E., Rha, C., Lemnitzer, A., Stewart, J.P., Taciroglu, E. and Wallace, J.W. (2014), "Nonlinear load-deflection behavior of reinforced concrete drilled piles in stiff clay", *J. Geotechnic. Geoenviron. Eng.*, **140**(3), 04013022.
- Kolozvari, K., Orakcal, K. and Wallace, J.W. (2014a), "Modeling of cyclic shear-flexure interaction in reinforced concrete structural walls. Part I: Theory", *J. Struct. Eng.*, **141**(5), 04014135.
- Kolozvari, K., Tran, T., Wallace, J.W. and Orakcal, K. (2015), "Modeling of cyclic shear-flexure interaction in reinforced concrete structural walls-Part II: Experimental validation", *J. Struct. Eng.*, **141**(5), 04014136.

- Kozmidis, A., Melek, M., Massone, L.M. and Orakcal, K. (2014), "Comparison of industry-standard nonlinear dynamic analysis methods with observed damage on a RC building", *Proceedings of the 10th U.S. National Conference on Earthquake Engineering*, Anchorage, USA.
- Lemnitzer, A., Khalili-Tehrani, P., Ahlberg, E.R., Rha, C., Taciroglu, E., Wallace, J.W. and Stewart, J.P. (2010), "Nonlinear efficiency factors for bored pile group under lateral loading", *J. Geotech. Geoenviron. Eng.*, ASCE, **136**(12), 1673-1685.
- Lemnitzer, Anne, Eric, R., Ahlberg, Alberto, Salamanca, Robert, Nigbor, Ertugrul, Taciroglu, John, Wallace and Jonathan, Stewart (2014), "Lateral load testing of a 2 ft. reinforced concrete fixed head single pile", Network for Earthquake Engineering Simulation (distributor), Dataset, doi: 10.4231/D3GQ6R33W.
- Li, Z., Kotronis, P. and Escoffier, S. (2014), "Numerical study of the 3D failure envelope of a single Pile in sand", *Comput. Geotech.*, **62**, 11-26.
- Martinelli, L. (2008), "Modeling shear-flexure interaction in reinforced concrete elements subjected to cyclic lateral loading", *ACI Struct. J.*, **105**(6), 675-684.
- Massone, L.M. (2010), "Strength prediction of squat structural walls via calibration of a shear-flexure interaction model", *Eng. Struct.*, **32**(4), 922-932.
- Massone, L.M. and Wallace, J.W. (2004), "Load - deformation responses of slender reinforced concrete walls", *ACI Struct. J.*, **101**(1), 103-113.
- Massone, L.M., Gotschlich, N.J., Kang, T.H.-K. and Hong S.-G. (2013), "Shear-flexural behavior and modeling of prestressed self-consolidating concrete beams", *Eng. Struct.*, **56**, 1464-1473.
- Massone, L.M., Orakcal, K. and Wallace, J.W. (2006), "Modeling flexural/shear interaction in RC walls", *ACI-SP-236*, Deformation capacity and shear strength of reinforced concrete members under cyclic loadings, American Concrete Institute, Farmington Hills, MI Paper 7, 127-150.
- Massone, L.M., Orakcal, K. and Wallace, J.W. (2009), "Modeling of squat structural walls controlled by shear", *ACI Struct. J.*, **106**(5), 646-655.
- Matlock, H. and Reese, L.C. (1970), "Correlations for design of laterally loaded piles in soft clay", *Proceeding of the 2nd Offshore Technology Conference*, OTC 1204, Houston.
- Mazars, J., Kotronis, P., Ragueneau, F. and Casaux, G. (2006), "Using multifiber beams to account for shear and torsion. Applications to concrete structural elements", *Comput. Meth. Appl. Mech. Eng.*, **195**(52), 7264-7281.
- Menegotto, M. and Pinto, E. (1973), "Method of analysis for cyclically loaded reinforced concrete plane frames including changes in geometry and non-elastic behavior of elements under combined normal force and bending", *Proceedings, IABSE Symposium*, Lisbon, Portugal.
- O'Neill, M.W. and Murchison, J.M. (1983), "An evaluation of p-y Relationships in sands", Research Rep. No. GT-DF02-83, Dept. of Civil Engineering, Univ. of Houston, Houston.
- OpenSees Development Team (Open Source Project) (1998-2009), OpenSees: Open System for Earthquake Engineering Simulation. <http://opensees.berkeley.edu>.
- Petrangeli, M. (1999b), "Fiber element for cyclic bending and shear of RC structures. II: Verification", *J. Eng. Mech.*, **125**(9), 1002-1009.
- Petrangeli, M., Pinto, P.E. and Ciampi, V. (1999a), "Fiber element for cyclic bending and shear of RC structures. I: Theory", *J. Eng. Mech.*, **125**(9), 994-1001.
- Ranzo, G. and Petrangeli, M. (1998), "A fibre finite beam element with section shear modelling for seismic analysis of RC structures", *J. Earthq. Eng.*, **2**(3), 443-473.
- Reese, L.C., Cox, W.R. and Koop, F.D. (1975), "Field testing and analysis of laterally loaded piles in stiff clay", *Proceeding of the 7th Offshore Technology Conference*, Dallas, Texas.
- Remino, M. (2004), "Shear modelling of reinforced concrete structures", Brescia, Italy: Ph.D. Dissertation, Dipartimento di Ingegneria Civile, Università degli Studi di Brescia, Italy.
- Saatcioglu, M. and Razvi, S.R. (1992), "Strength and ductility of confined concrete", *J. Struct. Eng.*, ASCE, **118**(6), 1590-1607.
- Scordelis, A.C. (1984), "Computer models for nonlinear analysis of reinforced and prestressed concrete structures", *PCI J.*, **29**(6), 116-135.
- Spacone, E., Filippou F.C. and Taucer, F.F. (1996), "Fibre beam-column model for nonlinear analysis of

- R/C frames: Part I. formulation”, *Earthq. Eng. Struct. Dyn.*, **25**(7), 711-725.
- Stewart, J.P., Taciroglu, E., Wallace, J.W., Ahlberg, E.R., Lemnitzer, A., Rha, C., Khalili-Teherani, P., Keowen, S., Nigbor, R. and Salamanca, A. (2007), “Full scale cyclic large deflection testing of foundation support systems for highway bridges. Part I: Drilled shaft foundations”, Report No. UCLA SGEL-01, University of California, Los Angeles.
- Taciroglu, E., Rha, C. and Wallace, J.W. (2006), “A robust macroelement model for soil-pile interaction under cyclic loads”, *J. Geotech. Geoenviron. Eng.*, **132**(10), 1304-1314.
- Thomsen, J.H. and Wallace, J.W. (2004), “Displacement-based design of slender RC structural walls-experimental verification”, *J. Struct. Eng.*, **130**(4), 618-630.
- Thorenfeldt, E., Tomaszewicz, A. and Jensen, J.J. (1987), “Mechanical properties of HSC and application in design”, *Proceeding of the Symp. On Utilization of HSC*, Stavanger, Norway.
- Tran, T.A. (2012), “Experimental and analytical studies of moderate aspect ratio reinforced concrete structural walls”, Ph.D. dissertation, Univ. of California, Los Angeles, USA.
- Vecchio, F.J. and Collins, M.P. (1988), “Predicting the response of reinforced concrete beams subjected to shear using the modified compression field theory”, *ACI Struct. J.*, **85**(3), 258-268.
- VirginiaATC-32 (1996), “Improved Seismic Design Criteria for California Bridges: Provisional Recommendations”, Applied Technology Council. <http://www.atcouncil.org/pdfs/ATC32toc.pdf>